

## A Very Wide-Field CCD Camera for Kiso Schmidt Telescope

Nobunari ITOH\*, Takao SOYANO\*, Ken'ichi TARUSAWA\*, Tsutomu AOKI\*, Sigeomi YOSHIDA\*,  
Takashi HASEGAWA†, Yasushi YADOMARU‡, Yoshikazu NAKADA\*,  
and Satoshi MIYAZAKI

(Received July 10, 2000)

### Abstract

A wide-field CCD camera has been manufactured for use on the 1.05m Schmidt telescope at Kiso Observatory. The camera makes use of a SiTe 2048×2048 CCD and has a wide field of view of 51'×51' with a pixel resolution of 1.5"/pixel at the prime focus of the telescope. The backside-illuminated CCD allows us to observe from 3500 Å to 1 μm. Fortunately, the shape of the CCD surface had a convex figure with very similar curvature to the focal plane of the Kiso Schmidt telescope, this coincidence helped us to avoid the field-flattener from the camera. Basic performances of the camera like the read-out noise were investigated.

Key words : instrumentation, imager, wide-field, CCD.

### 1. Introduction

A Schmidt telescope with large photographic plates, 6°×6° for the Kiso Schmidt, has been a powerful tool for survey studies. Schmidt plates such as POSS-I (Minkowski and Abell 1963), POSS-II (Reid et al. 1991) and SERC/ESO survey (Cannon 1983, West 1983) have provided fundamental and indispensable database in various kinds of astronomical fields. However, photographic plates have a severe problem of shallow detection limit. On the contrary, CCD detectors show a quantum efficiency more than twenty times higher than a photographic plate. In Kiso, Sekiguchi et al. (1992) developed a mosaic CCD camera, in which 2×8 1K-CCDs were arranged on the curved surface with the same curvature as that of the focal plane. The total area of the mosaic CCDs amounted to 0.7 square degrees. However, today's large format CCD covers a large field of view of 51'×51'(=0.7 square degrees) with just a single chip of an array detector. It is useless to say that a single image is better than the mosaic one for the astronomical purposes. Moreover, a back-illuminated CCD with reasonably high sensitivity in the UV wavelengths will be an ideal tool for the U band imaging. Fortunately, the corrector plate for the Kiso Schmidt is made of BSC7 which has more than 80%

transparency down to ~3300 Å. These advantages lead us to build a large format CCD camera for the Kiso Schmidt telescope. Although many kinds of observational studies are possible using the Schmidt telescope, some observations are particularly suitable to the large format CCD camera; (1) because the 17mm long spectra are obtained on the focal plane with the 4° objective prism the spectral observation needs a wide area of the large format CCD; (2) The large CCD fit well the dispersed configuration of open clusters; (3) the sky level is determined precisely only if we can spare a wide sky area surrounding the nearby apparently large galaxy; (4) a swiftly moving object can be paired when the image is taken twice with a sufficient interval; and (5) the multi-color photometric survey would be the most popular among the observations using a large CCD. To realize these observations at Kiso, we started the construction of the camera in 1996 and finished it in 1998. This instrument has been available for the visiting astronomers since 1998.

Here we report the performance of the new 2k×2k CCD camera and its application to the wide field imagings. We describe the system overview especially about the mechanics in section 2 and the data acquisition system and the electronics in section 3. The performance of the camera is summarized in section 4.

\* Kiso Observatory, the University of Tokyo

† Gunma Astronomical Observatory, Gunma

‡ Misato Observatory, Wakayama

## 2. Camera system

### 2.1 CCD Chip

The CCD chip is a SI424AB CCD chip, manufactured by SiTe Inc, USA. It has  $2048 \times 2048$  pixels each with a size of  $24 \times 24 \mu\text{m}$ . The imaging area is  $49 \times 49\text{mm}$  covering  $51' \times 51'$  with spatial resolution of  $1.5''$  per pixel at the prime focus of the Kiso Schmidt telescope. The CCD is backside-illuminated showing a significant sensitivity between the  $U$  band wavelengths and  $z$  band wavelengths. Only one readout channel is available for our CCD. There are two bad columns and several tens of bad pixels on our chip. The bad pixels account for 0.9% of all the pixels.

### 2.2 Dewar

The camera dewar has to be located at the prime focus of the Schmidt telescope. Only a limited space was available for the dewar because the photographic plate holder was just behind the focal point. The size of the dewar was, therefore, as small as  $186 \times 186 \times 100\text{mm}$ . The layout inside the dewar and its appearance from outside are shown in figure 1a and 1b. Since the camera was designed as an imager, the optical configuration inside the dewar was rather simple. The CCD chip was adhered to the cold surface using the Ag-based conductive epoxy (ECCOBOND 83C, Grace Japan). The cold surface was made of kovar, the same alloy as the CCD package, to minimize the thermal stress. The cold surface itself is mounted on a teflon base to isolate the heat

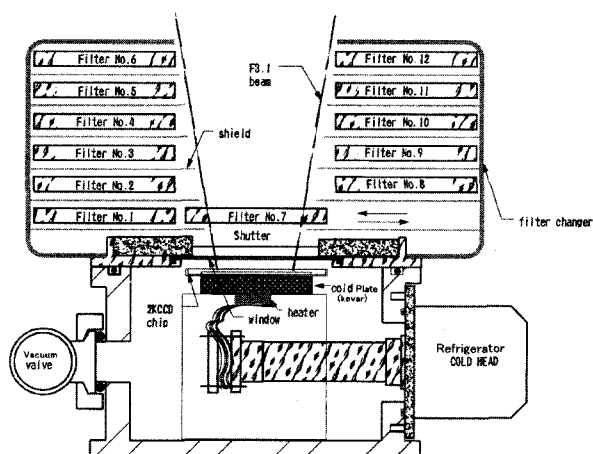


Fig. 1. a: A schematic view of our camera.

conduction from the wall of the dewar. It was cooled through a copper braid extending from the cold finger of a refrigerator.

A total thermal input into the dewar is about  $3.7\text{W}$  at  $-100^\circ\text{C}$  dominated by ( $\sim 80\%$ ) the radiation from the dewar window. The dewar is cooled by a compact refrigerator (Model s007; Iwatani co. Japan) whose cooling power is about  $20\text{W}$  at  $-100^\circ\text{C}$ . The refrigerator is connected to a compressor on the dome floor with two He sealed flexible tubes. The CCD chip is cooled down to  $-100^\circ\text{C}$  from the room temperature in 2.5 hours and the temperature is regulated within  $0.5\text{K}$  by the thermal controller (Model330; Lakeshore Cryotronics Inc.), which adjusts the electric current to the heater set under the cold surface. The vibration amplitude of the CCD chip due to the refrigerator is less than  $5 \mu\text{m}$  and its influence is negligible to the image quality.

The dewar window is of the size  $\phi 100\text{mm} \times t 1.1\text{mm}$  and is made of tempered glass, HOYA N50, with the AR coating to endure the atmospheric pressure. The glass allows more than 90% transmission of light within the wavelength range  $3500 \text{ \AA} \leq \lambda \leq 1 \mu\text{m}$ .

### 2.3 Convex CCD Surface

The curvature of the focal plane cannot be neglected for the Schmidt observations if one want to use a large format CCD. The focal plane of the telescope has the curvature of  $R/3300\text{mm}$  and the diagonal size of the CCD array is  $69.5\text{mm}$ . If a completely flat CCD was put on the focal point, the CCD edge would be  $180 \mu\text{m}$

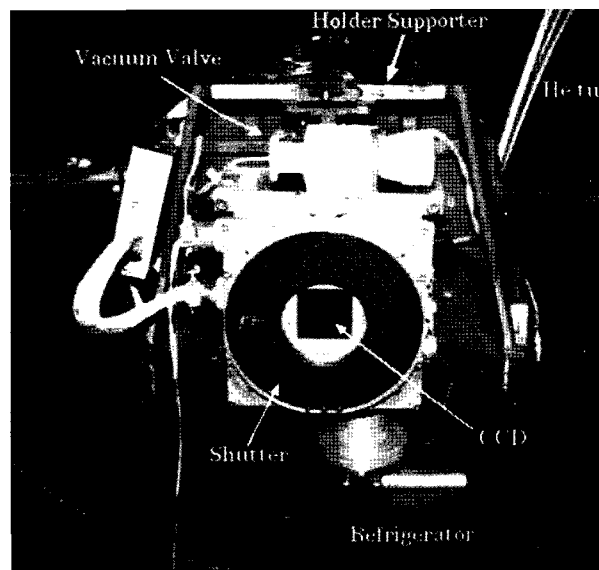


Fig. 1. b: Photograph showing our camera attached at the prime focus of Kiso Schmidt telescope. The picture was taken inside the telescope viewed from the primary mirror. The filter exchanger was not attached in this picture.

ahead from the curved focal plane. This discrepancy is much larger than the focal depth ( $50\ \mu\text{m}$ ) of the telescope. However, a surface of a former backside-illuminated CCD was known slightly convex because of a thinning process. Our solution to the curved focal plane was thus to choose a proper CCD chip whose surface curvature was very close to that of the focal plane. The CCD surface was measured at intervals of 7mm by a laser displacement sensor. The measurement error was about  $2\ \mu\text{m}$ . It was then compared with the curvature of the focal plane. Figure 2a shows the bird's-eye map of the CCD surface under the cooled condition. The origin of X-Y axes is located at the north-east corner of the CCD surface. The zero level of the Z-axis is arbitrary. The shape of the CCD surface looked almost spherical all over the imaging area. The peak-to-valley difference was about  $180\ \mu\text{m}$ , exactly the expected value for the focal plane. The vertical heights along the two diagonals of the CCD surface are dotted in figure 2b. The open circles indicate the height of the CCD surface along NE to SW direction and the open squares along SE to NW direction. The solid line shows the curvature of the focal plane. Apparently the CCD surface traces the curvature of the focal plane very well. The vertical differences between the CCD surface and the focal plane were less than  $10\ \mu\text{m}$  except for the NW corner where the CCD surface was  $20\ \mu\text{m}$  behind the focal point. Even the largest deviation at the NW corner is within the focal depth. The change of the CCD surface when it was cooled from the room temperature is shown in figure 2c. The curvature strengthened slightly when the CCD was cooled and the peak-to-valley was within  $16\ \mu\text{m}$ , but the change was negligibly small. The adhesion suppressed rise of the CCD due to the readout process to within 0.15K.

**2.4. Filter and Shutter**

The fast F/3.1 optics of the Kiso Schmidt telescope required large filters. A usual filter turret would lead to severe vignetting inside the telescope. Therefore, a rather unique design was adopted for the filter changer. Figure 3a and 3b show the inside of the changer and its enclosure. The changer had two filter rooms, each containing a stack of six filter holders. The status of each filter is detected by the micro switches. The scattered light was rejected or absorbed by the black-painted enclosure and by the partitions inside the filter rooms. It takes 7sec to exchange filters.

A  $\phi\ 80\text{mm}$  iris-type shutter is mounted in front of the camera window. It causes small differences in the exposure time among the pixel locations; a longer exposure

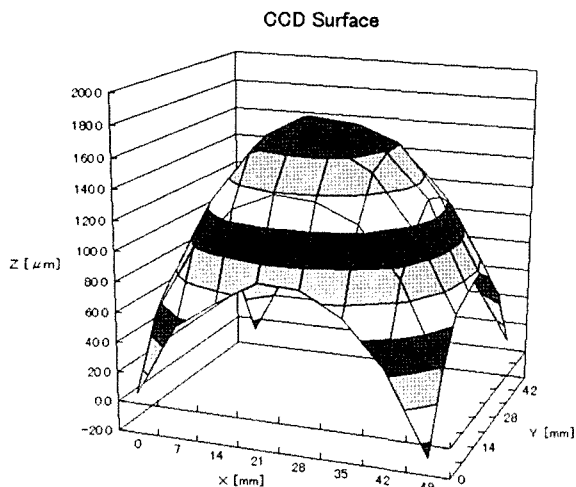


Fig. 2. a: The bird's-eye map of the CCD surface under the cooled ( $-100^\circ\text{C}$ ) condition.

The readout channel is correspond to the coordinate of  $(X,Y)=(0,49)$  and the origin of X-Y coordinates is correspond to the NE edge on a CCD image. The zero-level of the z-axis is arbitrary.

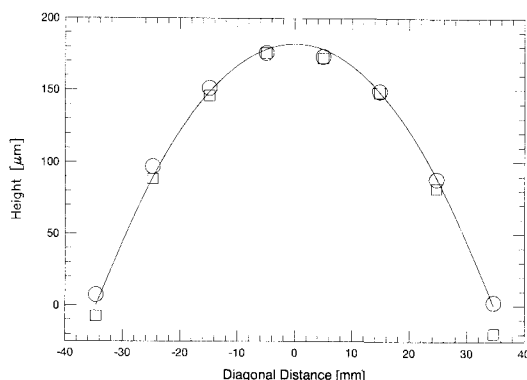


Fig. 2. b: The heights of the CCD surface along the diagonal direction. The open circles indicate the height of the CCD surface along NE to SW direction and the open squares along SE to NW direction. The solid line shows the curvature of the focal plane.

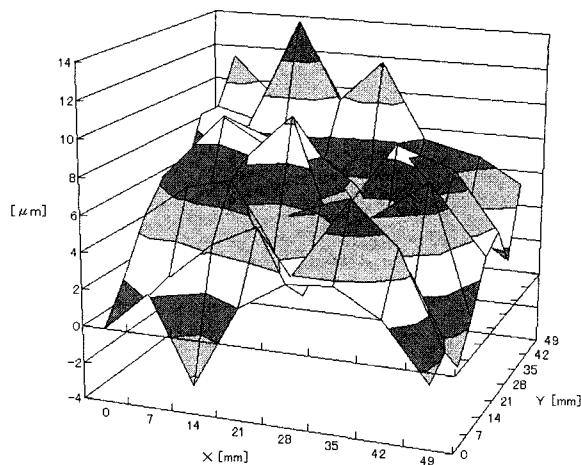


Fig. 2. c: The change of the CCD surface under the cooled condition from that under the room temperature. The peak-to-valley was within  $16\ \mu\text{m}$ .

time near the center than the corner. To keep this difference less than 1%, it is necessary to set the exposure time longer than 5 sec. The position of each filter is detected by micro switches to avoid overlap of filters on the light path.

### 3. Electronics and Data acquisition

#### 3.1 Data acquisition

The data acquisition system we adopted was MESSIA III developed by National Astronomical Observatory Japan. MESSIA, Modularized Expandable SyStem for Image Acquisition, is a universal array control system on VME bus and MESSIA III is its 3rd version (Sekiguchi et al. 1998). It consists of an S-Bus interface (SIF), a VME-memory interface (VMI), and a CCD and instrument controller (CIC). A schematic view of our data acquisition system is shown in figure 4. SIF is a FIFO buffer connected with VMI through an optical fiber link and is inserted in an S-Bus slot of a host workstation. The fiber link has an ability of 1Gbps data transfer. VMI can store 128Mbyte image data at its maximum and the read/write speed for the on-board frame memory is about 20Mbyte/sec. CIC has many I/O channels for both CCD and other instruments operation. CIC loads 32ch clock outputs for CCD operation and 2ch RS232C interfaces, 16bit PI/O, 8ch DAC/ADC interface, and so on. All I/Os can be controlled by a host workstation directly. We control a filter changer and a shutter through the CIC. The temperature controller is managed through RS-232C.

We provide over-scan regions which contain 10 pixels at one side and 7 pixels at another side of each horizontal line to monitor the bias level fluctuation. Image data are stored as FITS format and an image size is 8.4MB/frame.

#### 3.2. Electronics

Because of the diversity of detector types, MESSIA did not provide us with front-end electronics like a clock driver, a pre-amp, and an A/D converter which we had to make ourselves. A clock driver is a circuit to transform the clock signals to the appropriate clock voltages for CCD operation. Our clock driver has 24ch inputs, 24ch outputs, and 2ch DC power supplies. A photo-coupler (TLP2630) was set at each input channel to isolate electric noises from outside. Output voltage of each output channel is changeable within a range from  $-15V$  to  $+15V$ . The DC power channels supply constant voltages to the  $V_{DD}$  channels of a CCD and are adjustable in the range from  $0V$  to  $+25V$ . We adopted an analog switch (GD403) to change L/H levels of the operational volt-

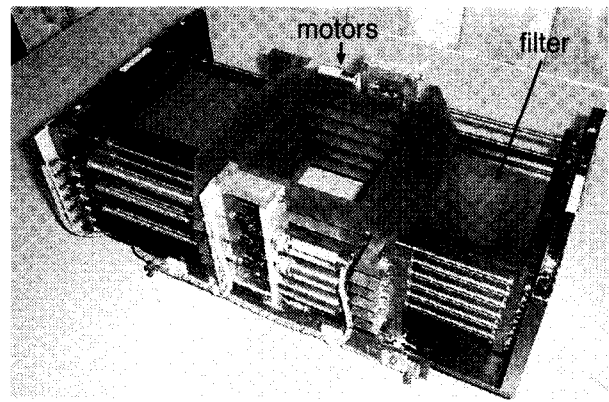


Fig. 3. a: The photograph of the filter exchanger. The filter exchanger has a capacity of six 100mm-square filters of each side, total of 12 filters. The position of each filter is detected by a pair of micro switches.

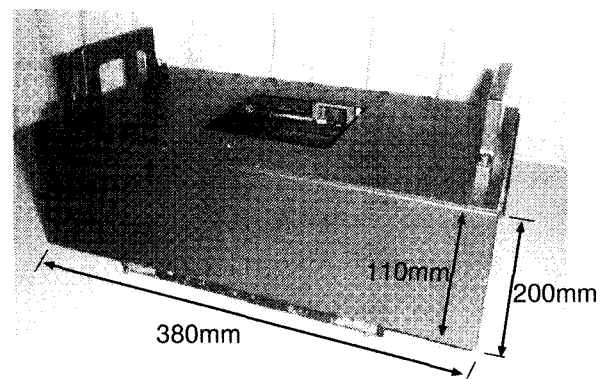


Fig. 3. b: The photograph of the exchanger attached a enclosure. The filter exchanger is mounted on the dewar in this style.

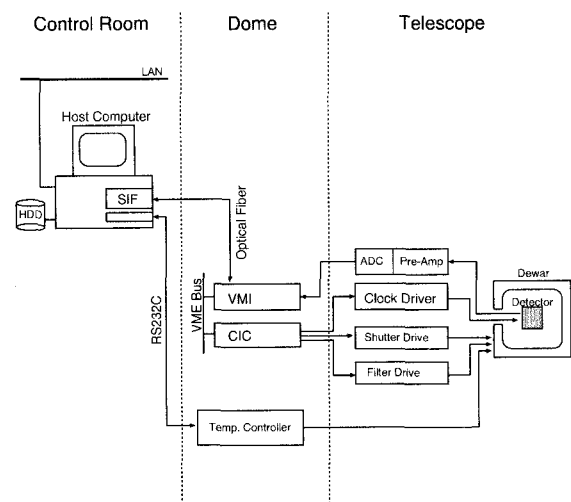


Fig. 4. The schematic view of our data acquisition system. The SBus interface (SIF), VME-memory interface (VMI), and CCD and instrument controller (CIC) constitute MESSIA. The clock driver, pre-amp, and ADC board, whose designs largely depend on the detector characteristics, were designed by ourselves. The camera is controlled by a workstation, Fujitsu S-4/5.

age. Output analog signals from the CCD are amplified by 10 times on the pre-amp board in the camera dewar. The output signals are then digitized by a 16bit A/D converter (CS510A) after passing a correlated-double sampling (CDS) circuit. The sampling and the conversion are synchronized with the clock signals. The digitizing frequency was tuned to  $50\text{kHz pixel}^{-1}$  to minimize the readout noise. With this frequency, the readout time was 95sec per 8.4MB. Four sets of CDS+ADC circuits were on a board to handle the 4ch signal outputs. The clock driver and the ADC board have double layers and a power supply is in common. The pre-amp, clock driver, and ADC boards were almost the same as those for mosaic CCD camera of the Sloan Digital Sky Survey (Gunn et al. 1998). Non-MPP operation was adopted for our system and the dark current was significantly low even under the non-MPP operation.

### 3.3 Control software

A Fujitsu S-4/5, Sparc station 5 compatible workstation serves as a host computer for the observation. With the help of the basic control commands provided by MESSIA III, we could develop the macro packages to operate the MESSIA commands successively. Since the macro package could also send commands of the telescope operation through the local area network, semi-automatic observations are possible by making macro files in which a series of commands on both the camera and the telescope operations are stored. The status information of the telescope and of the camera was automatically recorded in an image header of a FITS file. The remote access to the telescope is limited within the observatory for security.

## 4. Performance

The linearity of the output signal was investigated with a stabilized light source. The light intensity was changed by ND filters. We repeated the measurements four times for the high intensity experiments and three times for the low intensity ones. Signal counts are plotted against the exposure time for the different intensities in figure 5a, but all the four or three measurements with the same light intensity and exposure time are overlapped in the diagram and cannot be distinguished each other. The solid lines are the best fit curves for the two intensities by the assumed form of  $S = at^\gamma$ , where  $\gamma$  is a linearity index. The fitting was carried out in the range of  $5,000 \leq S \leq 30,000\text{ADU}$  simultaneously for the two intensities to derive the common value of  $\gamma$  as  $0.994 \pm 0.002$ . Fitting was tried with a linear relation too. Figure 5b shows the residual from the linear fit as a function of

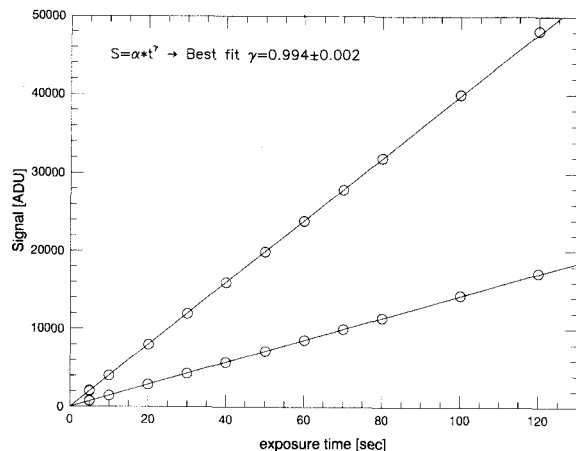


Fig. 5. a: Output signal plot as a function of exposure time. We took at least four frames at each exposure time. The solid lines indicate the best fit by the equation of  $S = at^\gamma$  and the fitting was carried out in the range of  $5,000 \leq S \leq 30,000\text{ADU}$ . The best fit value of  $\gamma$  was  $0.994 \pm 0.002$ .

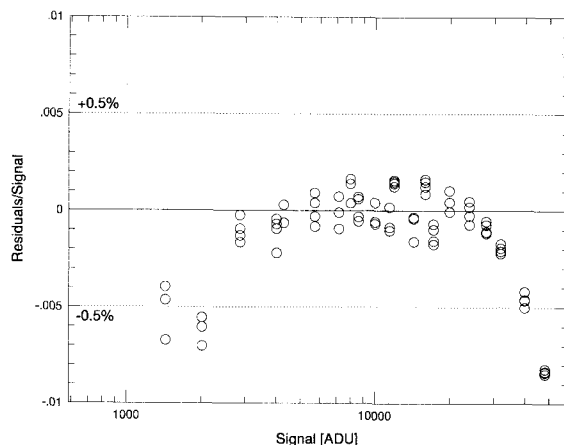


Fig. 5. b: The ratio of residuals from the best fit linear relation to the signal level. The fitting range of a linear equation was the same as (a). The dashed lines show  $\pm 0.5\%$  level. The lower and upper limits where the residuals from a linear assumption exceeds 0.5% were  $6,800e^- (=2,000\text{ADU})$  and  $100,000e^- (=30,000\text{ADU})$ .

a signal. It exceeds 0.5% at  $6,800e^- (=2,000\text{ADU})$  and  $100,000e^- (=30,000\text{ADU})$ . The  $100,000e^-$  corresponds to about 30% of full well capacity of a pixel.

The readout noise and the system gain of the camera were also measured in the same experiments. Figure 6 shows the noise against the signal in the logarithmic scale. The obtained system gain was  $3.4 \pm 0.1e^- / \text{ADU}$  and the readout noise was  $20.4 \pm 1.9e^-$  rms.

The charge transfer efficiency (CTE) was measured by the X-ray photon calibration technique using the Fe isotope (Luppino et al. 1987, Janesick et al. 1987). We

obtained the CTE as 0.999997 for the horizontal transfer and 0.999993 for the vertical one. This experiment also gave the system gain of  $3.6 \pm 0.2 e^-/\text{ADU}$ , consistent with the value obtained in the linearity experiment.

The total through-puts including the telescope optics were estimated by the observations of standard stars (Landolt 1982). They were 3%, 22%, 26%, 8% and 19% for  $U$ ,  $B$ ,  $V$ ,  $R_c$ ,  $I_c$  band, respectively. The low through-put of the  $R_c$  band was caused by the low transparency of our  $R_c$  filter. The  $U$  band through-put of our camera is three times higher than that of Kiso 1K CCD camera and it is feasible to perform the spectroscopic observations with the  $4^\circ$  prism around  $4000 \text{ \AA}$  (Kanya and Jugaku 2000).

#### 4.1. System Stability

The CCD temperature deviates slightly by  $0.3 - 0.6 \text{ K}$  during a night and it indicates a rough correlation with the atmospheric temperature. The half period of the typical temperature fluctuation is about 8–10 hours. The bias level shows a loose anti-correlation with the CCD temperature as shown in figure 7 and its slope is  $-28 \text{ ADU/K}$ . Accordingly, the bias level may change as much as  $15 \text{ ADU}$  during a night. No correlation was found between the elevation of the telescope and the bias level.

Dark current was negligible ( $< 1 e^- \text{ pixel}^{-1} \text{ hour}^{-1}$ ) under the operating temperature ( $\sim -100^\circ \text{ C}$ ).

#### 4.2. Image Quality

Thanks to the curved surface of the CCD chip, this camera does not need a field-flattener. Although we have confirmed that the shape of the CCD surface was very similar to the focal plane, it was necessary to investigate the actual image quality of stars on the CCD surface. Therefore, the CCD array was divided into  $3 \times 3$  blocks, each having  $600 \times 600$  pixels, and the FWHMs were measured using the Gaussian fit to individual images. The stellar size was estimated with FWHMs of Gaussian fit. Figure 8 shows an example of stellar size distributions. The abscissa of each histogram is the stellar FWHMs in arcsec and the ordinate is the number of stars. Each histogram is allocated according to the location of each block on the CCD; the bottom-left corresponds to the south-east on the CCD and the top-right to the north-west. Each block has  $600 \times 600$  pixels and at least 300 stars were measured in each block.

The average stellar size over the whole area was  $3.1''$ , a typical seeing size at Kiso, and is indicated as dashed lines in the histograms. All the blocks but one at

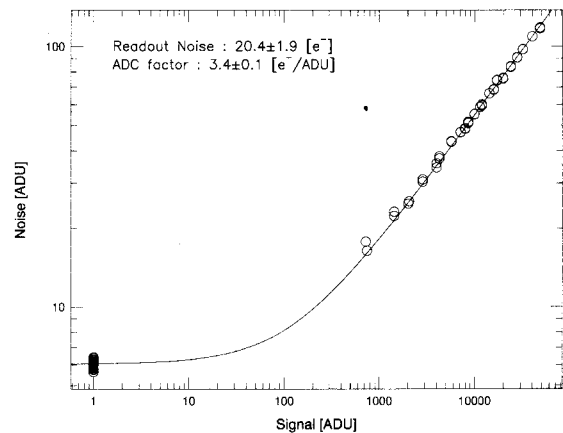


Fig. 6. A signal-variance plot. The data were taken with a stabilized light source and signal level was controlled by changing an exposure time. The solid line shows the result of a least square fitting. The obtained system gain is  $3.4 \pm 0.1 e^-/\text{ADU}$  and readout noise is  $20.4 \pm 1.9 e^-$ .

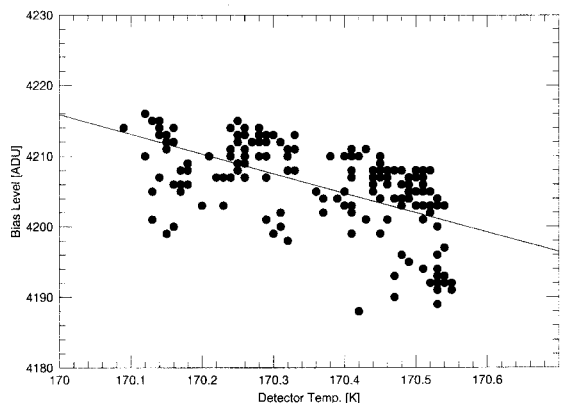


Fig. 7. The bias level against the detector temperature. The bias levels were measured at the overscan regions and had a loose anti-correlation with the detector temperature. The solid line shows the regression line and its slope was  $-28 \text{ ADU/K}$ .

the NW corner show the similar size distribution. The average stellar size for the NW block was about 8% larger than other blocks. The large deviation of the NW corner from the focal plane is probably responsible for the wider stellar images there. As we showed in figure 2b, the CCD surface deviated from the ideal focal plane the most at the NW corner. The large deviation of  $20 \mu\text{m}$  there can explain the extended image.

#### 4.3. Fringe Pattern

A significant fringe pattern appears on our  $I_c$  image. This was the common phenomena, an interference of the air glow light inside the CCD chip, to the backside-illuminated CCD. The strength of fringe patterns change day by day and the typical amplitude is about

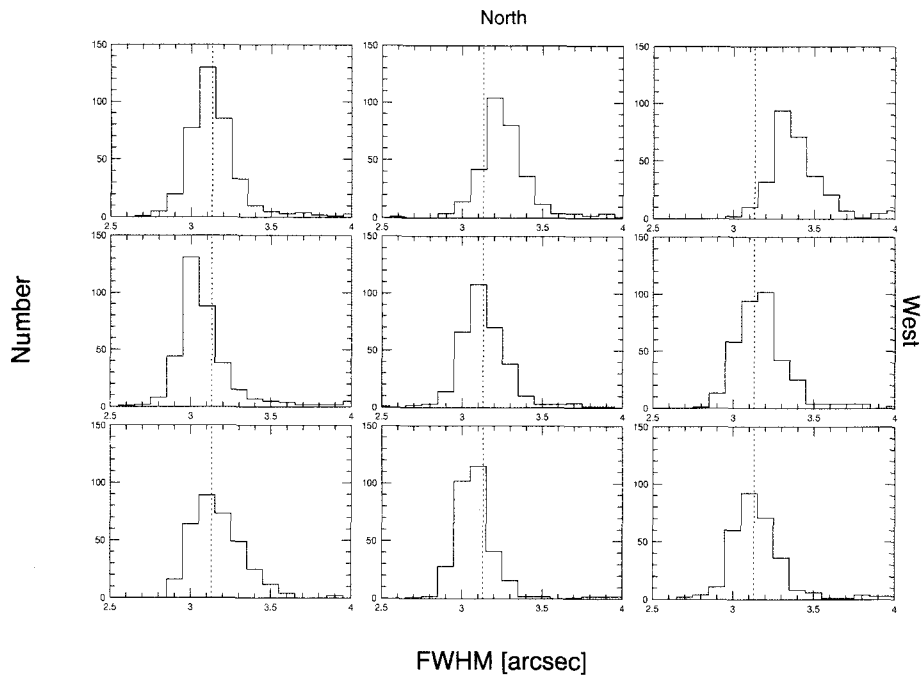


Fig. 8. The stellar imaging size (FWHM) distribution. The abscissa of each histogram shows seeing size and the ordinate is the number of stars. The location of each graph is correspond to the area on the CCD, that is, the bottom-left correspond to the south-east on the CCD and the top-right to the north-west. The image used here was taken in  $I_C$  band with 120sec exposure. The stellar size was estimated with FWHMs of Gaussian fit. The average stellar size over whole image area was  $3.1''$  and is indicated as dashed lines in the histograms. The  $3''$  seeing is typical seeing condition at Kiso. The systematic differences about the stellar size distribution were not found among the blocks except for the north-west (NW) block. The average stellar size at NW block was about 8% larger than other blocks.

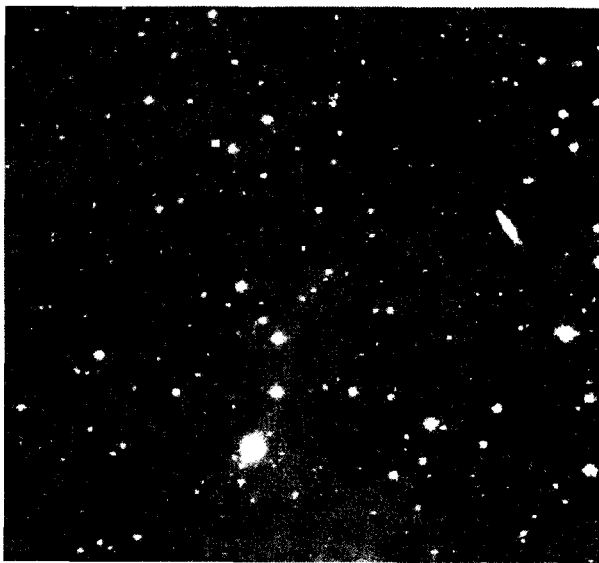


Fig. 9. An Example of fringe removal.  
a: This image was taken in  $I_C$  band with 360sec exposure and The image area is the central  $500 \times 500$  pixels. The fringe amplitude is about 1% of the sky level.

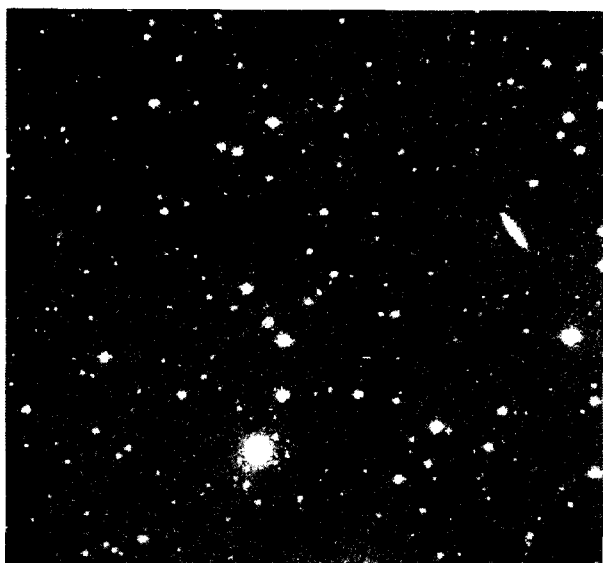


Fig. 9. b: An image after fringe removal by adaptive modal filtering. The fringe pattern is reduced until 0.3% of the sky level.

0.8% of the sky level at  $I_c$ . We confirmed that the adaptive modal filtering routine (McLean 1997) removed fringes to the considerably low level of 0.3 to 0.5%. Figure 9 shows the removal of the fringe patterns by this method. In this case, a fringe pattern was reduced down to 0.3% level.

## 5. Summary

We have constructed a wide-field imaging camera equipped with a single  $2048 \times 2048$  CCD array detector for the Kiso Schmidt telescope. The camera has a  $51' \times 51'$  field of view with  $1.5'' \text{pixel}^{-1}$  resolution on the prime focus. This wide field of view combined with a high through-put of the optics made this camera particularly suitable for the wide-field surveys and individual observations of large scale objects. We have made use of the convex surface of the detector to avoid the field-flattener for the large format CCD. The image qualities were found nearly the same all over the imaging area.

The camera has significant throughput in the ultraviolet. Accordingly, we can observe objects from  $U$  to  $z$  band. The camera has been available to the common users of the Kiso Observatory since 1998.

## References

- Cannon, R. D., 1984, IAU coll. vol. 78, p.25.
- Gunn, J. E. et al., 1998, *Astron. J.*, **116**, 3040.
- Hayashino, 1999, private communication.
- Janesick, J., Elliot, T., Collins, S., Blouke, M., and Freeman, J., 1987, *Optical Engineering*, **26**, 692.
- Kanya, Y. and Jugaku, J., 2000, private communication.
- Luppino, G. A., Ceglio, N. M., Doty, J. P., Ricker, G. R., and Vallergera, J. V., 1987, *Optical Engineering*, **26**, 1048.
- Luppino, G. A. and Miller, K. R., 1992, *Publ. Astron. Soc. Pac.*, **104**, 215.
- Luppino, G. A., Tony, J. L. and Stubbs, C. W., 1998, *SPIE*, **3355**, 469.
- McLean, I. S., 1997, *Electric Imaging in Astronomy*, John Wiley & Sons Ltd.
- Minkowski, R. and Abell, G. O., 1963, *Stars and Stellar System*, **3**, Basic Astronomical Data, ed. K. A. Strand, Chicago: Univ. of Chicago Press, 1963, p.481.
- Reid, I. N., Brewer, C., Brucato, R. J., McKinley, W. R., Maury, A., Mendenhall, D., Mould, J. R., Muller, J., Neugebauer, G., Phinney, J., Sargent, W. L., Schombert, J. and Thicksten, R., 1991, *Publ. Astron. Soc. Pac.*, **103**, 661.
- Sekiguchi, M., Iwashita, H., Doi, M., Kashikawa, N. and Okamura, S., 1992, *Publ. Astron. Soc. Pac.*, **104**, 744.
- Sekiguchi, M., Nakaya, H., Kataza, H., and Miyazaki, S., 1998, *Optical Detectors for Astronomy*, eds. J. W. Beletic and P. Amico, Dordrecht: Kluwer, 1998, p.157.
- West, R. M., 1984, IAU coll. vol. 78, p.13.